Available online at www.sciencedirect.com
ScienceDirect
Journal of Nuclear Materials 366 (2007) 388–406
journal of nuclear materials
www.elsevier.com/locate/jnucmat

Radiation-damage in molybdenum–rhenium alloys for space reactor applications

J.T. Busby *, K.J. Leonard, S.J. Zinkle

Materials Science and Technology Division, Oak Ridge National Laboratory, P.O. Box 2008, Oak Ridge, TN 37831-6132, United States

Abstract

Various Mo–Re alloys are attractive candidates for use as fuel cladding and core structural materials in spacecraft reactor applications. Molybdenum alloys with rhenium contents of 41–47.5% (wt%), in particular, have good creep resistance and ductility in both base metal and weldments. However, irradiation-induced changes such as transmutation and radiation-induced segregation could lead to precipitation and, ultimately, radiation-induced embrittlement. The objective of this work is to evaluate the performance of Mo–41Re and Mo–47.5Re after irradiation at space reactor relevant temperatures. Tensile specimens of Mo–41Re and Mo–47.5Re alloys were irradiated to ~0.7 displacements per atom (dpa) at 1073, 1223, and 1373 K and ~1.4 dpa at 1073 K in the High Flux Isotope Reactor at Oak Ridge National Laboratory. Following irradiation, the specimens were strained to failure at a rate of 1×10^{-3} s^{-1} in vacuum at the irradiation temperature. In addition, unirradiated specimens and specimens aged for 1100 h at each irradiation temperature were also tested. Fracture mode of the tensile specimens was determined. The tensile tests and fractography showed severe embrittlement and IG failure with increasing temperatures above 1100 K, even at the lowest fluence. This high temperature embrittlement is likely the result of irradiation-induced changes such as transmutation and radiation-induced segregation. These factors could lead to precipitation and, ultimately, radiation-induced embrittlement. The objective of this work is to examine the irradiation-induced degradation for these Mo–Re alloys under neutron irradiation.

PACS: 61.80.Hg; 61.82.Bg; 62.20.Fe; 89.30.Gg; 81.05.Bx

1. Introduction

Almost every new, high-temperature reactor design begins by specifying unalloyed Mo or dilute Mo-based alloys as the reference structural material due to their high melting points, good thermal properties and excellent high temperature strength. However, in most cases, other candidate materials replace these Mo-based alloys because of difficulties associated with fabrication, low room-temperature ductility, and the high degree of embrittlement observed after irradiation. Molybdenum–rhenium (Mo–Re) alloys have been suggested for use in a number of high temperature nuclear reactor applications, such as fuel cladding and structural components, because they possess good thermal and mechanical properties while being easier to fabricate than unalloyed Mo. Two alloys (with 41 and

* Corresponding author. Tel.: +1 865 241 4622; fax: +1 865 241 3650.
E-mail address: busbyjt@ornl.gov (J.T. Busby).

0022-3115/$ - see front matter © 2007 Elsevier B.V. All rights reserved.
doi:10.1016/j.jnucmat.2007.03.028

47.5 wt% Re) are particularly attractive for spacecraft reactor applications [1]. These two alloys are more expensive and dense than unalloyed Mo, but possess better ductility, mechanical properties, thermal properties, and fabrication properties [2–8]. However, some gaps in the database still exist.

One of the most important factors in assessing potential materials for nuclear power applications is the material performance under neutron irradiation. Unfortunately, there are only a few studies available in the open literature on the irradiation-performance of these alloys. Fabrietsiev and Pokrovsky [9] examined the tensile properties in Mo–Re alloys irradiated over a range of temperatures in either the mixed spectrum of the SM-2 reactor or the fast spectrum of the BOR-60 reactor. Severe embrittlement and brittle fracture were observed in the 573–873 K temperature regime. Some limited ductility was retained for irradiations and tests between 973 and 1073 K. Hasegawa et al. [10] found that a Mo–5Re alloy irradiated in FFTF at 546–1073 K also exhibited a very high degree of hardening and loss of ductility, but did not undergo brittle fracture. The data of these two studies are consistent, leading to the belief that the minimum operating temperature for Mo–Re alloys to avoid low temperature radiation embrittlement is ~1100 K. However, no data exists for temperatures above 1100 K.

The purpose of this paper is to evaluate the response of Mo–Re alloys (Mo–41Re and Mo–47.5Re) to irradiation at spacecraft reactor relevant temperatures (1073–1373 K) up to 1.4 displacements per atom (dpa). While this dose may not represent the expected damage level for a space reactor component at the end of life, it does provide key information on irradiation-induced degradation of this alloy system. The results of tensile testing on samples irradiated at 1073–1373 K to 0.7 and 1.4 dpa are presented, along with fractography on the fracture surface. Finally, the potential impact of radiation-induced segregation and transmutation on embrittlement is presented.

2. Experimental procedures

Two Mo–Re alloys (Mo–47.5Re and Mo–41Re) were examined in this study. The Mo–47.5Re alloy was made via powder-metallurgy techniques and was provided by Pittsburgh Materials Technology, Inc. (PMTI). The Mo–41Re alloy was produced at Oak Ridge National Laboratory (ORNL) via vacuum arc-remelting. The chemical compositions for each alloy are shown in Table 1.

Tensile specimens were fabricated from the as-received sheet material using wire electrical discharge machining (EDM). The SS-3 sample geometry was chosen (a schematic of the SS-3 specimen is shown in Fig. 1). The Mo–41Re material was provided in 0.018 in. (0.45 mm) thick sheet. The Mo–47.5Re was provided in a bar form and samples were cut to 0.03 in. (0.76 mm) thick using EDM. The wire EDM process used only Mo-wire to minimize impurity pickup during machining. Further, only water was used as a coolant instead of cutting oil. Specimens were cut so that the long direction of the gage section was along the rolling direction of the sheet material. After sample fabrication and prior to annealing, all samples were electrochemically cleaned in a solution of nitric acid, phosphoric acid, hydrofluoric acid, and acetic acid for one minute. All samples were then annealed for 1 h at 1773 K in vacuum (better than 5×10^{-6} Torr).

2.1. Sample irradiation

A total of six capsules were constructed for irradiation in HFIR PTP positions in order to irradiate to two damage levels at three different temperatures. The capsules were irradiated for either one or two cycles in HFIR cycles 404, and/or 405 in the midplane positions (positions 4 and 5). While the same position was not used for each capsule, each position was selected to minimize differences in spectra and flux. The accumulated fluence for each capsule is summarized in Table 2, along with the thermal, epithermal, and fast neutron contributions. Dose was calculated using a conversion factor of 2.78×10^{21} n/cm^2 ($E > 0.1$ MeV) per dpa [11]. This results in a range of doses between 0.66 and 1.46 for the samples of this study.

Four samples of each alloy were included in each capsule. Each capsule was designed to balance the reactor gamma heating and heat flow across a controlled thermal gap to achieve the desired irradiation temperature. Varying the radius of an unalloyed Nb specimen holder controlled the thermal gap conductance and thus, the gap between holder and the aluminum housing. Niobium was chosen for the holder as it is also a refractory metal with a suitably high melting temperature. Thermal gap conductance was also adjusted by varying the fill gas for the capsule. Heat transferred across the gap and through the capsule was removed by the

Table 1
Chemical composition of alloys (in wt% or wppm)

Alloy	Mo	Re	Nb[a]	Zr[a]	Hf[a]	Ta[a]	C[a]	O[a]	H[a]	N[a]
Mo–47.5Re	52.8	47.2	<50	<50	<50	<50	32	<50	<3	<20
Mo–41Re	58.1	41.9	<50	<50	<50	<50	<20	<20	<50	<3

[a] In wppm.

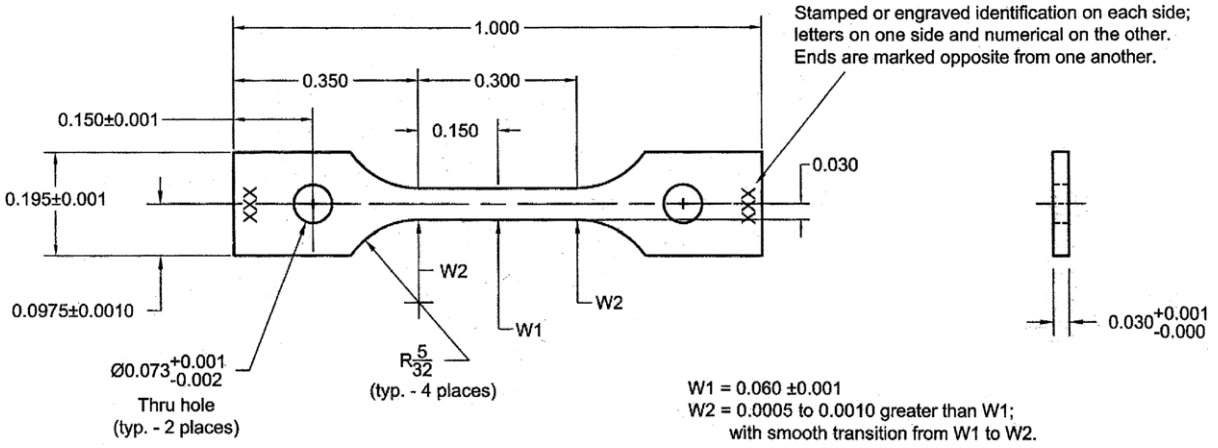

Fig. 1. Schematic of the SS-3 specimen. All dimensions are in inches.

Table 2
Fluence for each individual capsule

Capsule ID	Irradiation temperature (K)	HFIR cycles	Fluence ($\times 10^{21}$ n/cm^2)				
			Thermal	Epithermal	Fast		
			$E < 0.5$ eV (n/cm^2)	E 0.5 eV–0.1 MeV (n/cm^2)	$E > 0.1$ MeV (n/cm^2)	Total (n/cm^2)	Damage level (dpa)
J05-PF05	1073	404	3.37	2.42	2.00	7.80	0.72
J05-PF06	1073	404, 405	6.84	4.91	4.06	15.8	1.46
J05-PF11	1223	405	3.76	2.07	1.92	7.75	0.69
J05-PF17	1373	405	4.69	1.50	1.85	8.03	0.66

reactor cooling water. Helium was used as the fill gas for irradiations at 1073 and 1223 K, while neon was used for the irradiations at 1373 K. The purity of the both fill gasses was 99.999%. The radius of each Nb-holder was calculated for each loading configuration (alloys, number of samples, desired temperature, and planned core location) and machined to a tolerance of ±0.0003 in. (0.00762 mm). In addition to the samples, passive temperature monitors were also placed inside each capsule. The samples and temperature monitors were held in place by unalloyed Mo springs. More details about the design and construction of these HFIR irradiation capsules can be found in Ref. [12].

As noted above, the actual irradiation temperature was determined using passive SiC thermometry, which has been used as a passive irradiation temperature monitoring method since 1961. The post-irradiation evaluation of SiC temperature monitors used in this study is discussed in more detail in [13]. At the time of this publication, one set of thermometry has been completely analyzed. The thermometry for the capsule irradiated at 1073 K for one cycle has been completed. The thermometry indicates that the sample temperature was only 15 K higher than the target temperature of 1073 K. While the thermometry analysis has not been completed for the other Mo–Re irradiation

capsules, there is confidence that the actual irradiation temperatures will be in good agreement with the target temperatures as all the Mo–Re capsules used the same design criteria and heat generation rates.

In addition to the irradiated samples, unirradiated and thermally-aged control specimens of both alloys were also tested. Samples of both alloys were aged at the same temperature and fill gas for the same elapsed time as the HFIR irradiations. These specimens can provide information that helps separate irradiation-produced and thermally-induced changes in an alloy. In order to provide the most valid comparison to the HFIR irradiations, the individual tensile specimens (size SS-3) were loaded into spare HFIR rabbit capsules made of unalloyed Nb and secured with Mo springs in the same geometry used for the irradiation capsules. Strips or tabs of identical material were also included in the aging studies to provide specimens for the optical metallography and TEM studies which are part of a companion study [14].

Aging treatments were performed in sealed Alloy 600 cans placed in high temperature furnaces with an air environment. The samples were aged at 1098, 1248, or 1398 K. The aging temperatures are 25 K higher than the designed irradiation temperatures for the HFIR capsules. This temperature selection was made for conservatism, relative to the margin of uncertainty in the design irradiation temperatures. Aging treatments were for 1100 h (46 days), which is the approximate time at power of two cycles in HFIR.

2.2. Tensile testing and fractography

Tensile testing was performed on the as-irradiated and control SS-3 specimens using the ASTM standard E8, 'Standard Test Method for Tension Testing of Metallic Materials' [15]. Yield stress, ultimate tensile stress, and uniform and total elongation were determined for each test.

Tests were performed in a United Technology System SFM-10 with a Thermal Technology vacuum furnace, which is capable of reaching a test temperature of 1873 K (1600 °C) and a vacuum of 10^{-6} Torr or better by employing molybdenum heating elements and a turbo-molecular pumping system. A load cell with 2200 N (500 lbf) capacity was used, which is integrated in the load train and placed in the water-cooled zone of the vacuum chamber below the hot zone of the furnace. This feature eliminates the need to compensate for vacuum and bellow seal loading factors, thus the load cell directly measures the load applied to the test specimen. Tensile testing was performed at a crosshead speed of 0.0076 mm/s (0.018 in/min), corresponding to a nominal strain rate of $\sim$0.001 s^{-1}. Testing of the aged and irradiated specimens was performed at the same temperature as irradiation (1073, 1223, or 1373 K).

Following tensile testing, fractography was performed on select specimens using a TopCon ABT32 model scanning electron microscope. The nature of failure (intergranular (IG), transgranular (TG), ductile, or mixed) was assessed for each specimen. In addition, the percent IG was also measured when applicable. The reduction in area (RA) of the fractured specimen was also determined to provide an additional measure of ductility to complement the measured uniform elongation.

3. Results

Tensile testing of Mo–47.5Re and Mo–41Re was performed on the samples irradiated at 1073 K to 0.72 dpa, 1073 K to 1.46 dpa, 1223 K to 0.69 dpa, and at 1373 K to 0.66 dpa. In addition, fractography was completed on these fractured samples, in order to give a complete description of the mechanical performance. The results of the tensile tests on the aged, annealed, and irradiated specimens are presented for each alloy. However, due to limited space, the stress–strain curves and fractography for each individual specimen are not shown here, but are presented elsewhere [16].

3.1. Mo–47.5Re

A total of 17 tensile tests were completed on the Mo–47.5Re alloy. The tensile results are summarized in Table 3. Fractography was been performed on a majority of the Mo–47.5Re specimens and the quantitative results are also listed in Table 3.

3.1.1. Tests at 1073 K

The stress–strain curves for the annealed, irradiated, and aged specimens tested at 1073 K are shown in Fig. 2. The aged specimens show a slight increase in strength over the annealed condition, consistent with the room temperature hardness results obtained from the same specimens [14].

Two specimens of Mo–47.5Re irradiated at 1073 K to 0.72 dpa were tested. After the first

Table 3
Tensile properties of Mo–47.5Re

Test temperature (K)	Sample	Condition	YS (MPa)	UTS (MPa)	Uniform elongation (%)	Total elongation (%)	Failure location	Failure type[a]	Reduction area (%)	IG/TG Fracture (%)
RT	R727	Annealed	561	893	17.4	19.9				
1073	R728	Annealed	270	510	15.3	25.0	Gage	Ductile	83.9	0
	R731	Aged (1098 K)	284	525	16.5	24.1				
	R732	Aged (1098 K)	278	513	16.3	28.2				
	R733	Aged (1098 K)	269	508	21.8	29.6	Gage	Ductile	80.4	0
	R705	Irradiation (1073 K/0.72 dpa)	1370	1720	5.3	8.3	Gage	IG/TG	9.8	52.1
	R706	Irradiation (1073 K/0.72 dpa)	1030	1480	6.9	9.1	Gage	IG/TG	16.1	50.8
	R709[b]	Irradiation (1073 K/1.46 dpa)	920	1304	9.2	11.0	Gage			
	R712[c]	Irradiation (1073 K/1.46 dpa)	–	1081	–	–	Holes			
1223	R754	Annealed	300	464	15.1	29.6				
	R734	Aged (1248 K)	277	481	19.3	38.3	Gage	Ductile	77.7	0
	R735	Aged (1248 K)	262	442	15.4	36.1				
	R701	Irradiation (1223 K/0.67 dpa)	1180	1500	4.3	4.3	Gage	IG	10.0	100
1373	R725	Annealed	223	326	14.5	62.9	Gage	Ductile	89.2	0
	R737	Aged (1398 K)	275	367	8.8	34.8	Gage	Ductile	69.8	0
	R738	Aged (1398 K)	239	325	7.5	32.8				
	R717	Irradiation (1373 K/0.66 dpa)	526	896	4.4	4.4	Gage	IG	2.9	100

[a] Failure type given as ductile, intergranular (IG), transgranular (TG), or mixed (IG/TG).
[b] Loading pins bent during test. UE and TE could be up to 8.3% lower than reported value.
[c] Sample failed before yielding.

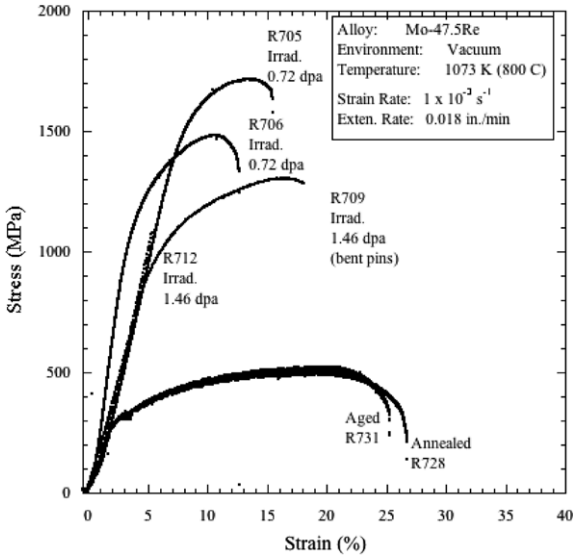

Fig. 2. Comparison of stress–strain curves for irradiated, aged, and annealed Mo–47.5Re at 1073 K.

sample (R706) was tested, it was found that the Mo loading pins were bent during testing. The bending of the pins was likely due to the unexpectedly high strength of the irradiated specimen (with a yield strength over 1 GPa). This deflection of the loading pins influences the measured YS, UE, and TE of the sample and following the test, the amount of bending in the pins was measured. The stress strain curve was corrected by subtracting this amount of extension (0.025 in. or 0.64 mm). The corrected curve is shown in Fig. 2 and the revised total elongation of 9.1% is very close to the actual total elongation measured on the fractured specimen.

Two specimens of Mo–47.5Re irradiated at 1073 K to 1.46 dpa were also tested and the stress–strain curves are shown in Fig. 2. Upon unloading the sample R709, these loading pins were, again found to be bent. Unfortunately, the amount of deflection on the pins could not accurately be measured and the actual UE and TE could be up to 8.3% lower than the values reported in Table 3. For the remainder of the tensile tests on the Mo–Re, stronger Mo–47.5Re pins were used. The second sample (R712) irradiated to 1.46 dpa at 1073 K failed prior to yielding with no plastic deformation, as shown in Fig. 2. The maximum stress for this specimen was 1081 MPa. This sample was observed to have failed at the hole in the end of the specimen rather than the gage section upon removing the sample from the tensile testing machine, indicating a highly embrittled failure, although no confirmatory fractography has been performed.

The fractography results summarized in Table 3 highlight the pronounced differences in the irradiated mechanical behavior from the aged and annealed Mo–47.5Re, consistent with the tensile properties and stress–strain curves. The fracture surfaces of the Mo–47.5Re specimens tested at 1073 K are compared in Fig. 3. Both the aged and annealed specimens show the expected ductile-dimple behavior. However, the fracture surface of the irradiated sample R705 is significantly different. The reduction of area for this specimen was only 9.8%. Intergranular facets are clearly visible even at low magnifications and the fracture surface of this specimen was found to be 52% IG. The IG facets are relatively uniformly distributed over the entire fracture surface instead of being concentrated at one side or corner of the specimen. There are also small amounts of localized dimpling located between the IG facets. This result suggests that after 0.7 dpa at 1073 K, the alloy is near the end of the transition from ductile/dimple to brittle IG fracture. The fracture surfaces of the samples irradiated at 1073 K to 1.46 dpa must be examined to confirm this trend.

3.1.2. Tests at 1223 K

Samples in the as-annealed and irradiated conditions have been tested at 1223 K. Two Mo–47.5Re samples aged at 1248 K for 1100 h have also been tested. The stress–strain curves for the annealed, aged, and irradiated specimens are shown in Fig. 4. In contrast to tests at 1073 K, aging at 1248 K resulted in a decrease in YS when compared to the as-annealed sample, which may, in part, be related to specimen-to-specimen variability. However, the UTS and UE are similar in the aged and annealed specimens. The TEM analysis performed on the aged specimens indicates that a nearly continuous chi phase, χ, has formed along the grain boundaries [14].

A sample irradiated to 0.69 dpa at 1223 K has also been tested and showed a large increase in strength over the annealed and aged control specimens, as expected. The differences in stress–strain curves were similar to those observed for the samples irradiated at 1073 K, and are also shown in Fig. 4. Like the samples irradiated at 1073 K, there is also a corresponding decrease in ductility. Further, the sample irradiated to 0.69 dpa (R701) fails

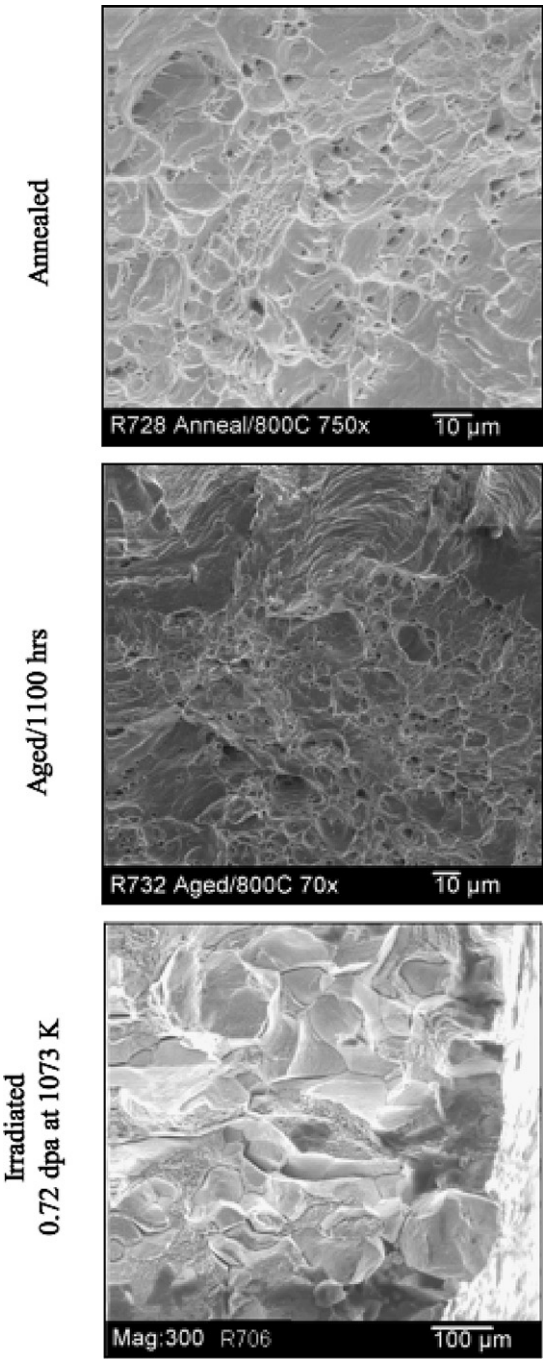

Fig. 3. Comparison of fracture surface of annealed, aged, and irradiated (0.72 dpa) Mo–47.5Re samples tested at 1073 K.

abruptly after only 4.3% strain with the total elongation equal to the uniform elongation, indicative of highly embrittled grain boundaries.

The fracture surface for the aged condition (sample R734) showed no signs of IG failure with a reduction in area over 77%. However, the irradiated sample has very little reduction in area (10%) and the fracture surface is completely IG. This observation will be discussed in more detail in a later section.

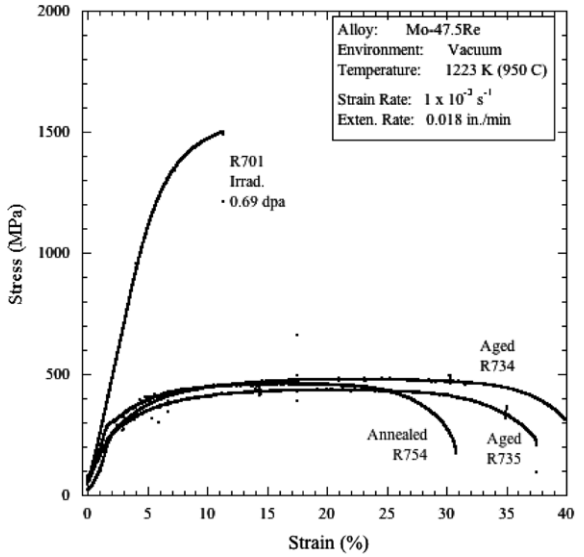

Fig. 4. Comparison of stress–strain curves for irradiated, aged, and annealed Mo–47.5Re at 1223 K.

3.1.3. Tests at 1373 K

An annealed, two aged, and an irradiated Mo–47.5Re specimen have been tested at 1373 K. The stress–strain curves are compared in Fig. 5. Again,

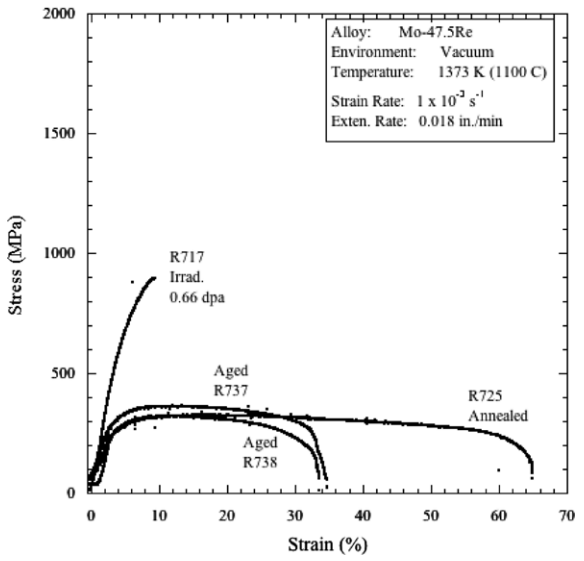

Fig. 5. Comparison of stress–strain curves for irradiated, aged, and annealed Mo–47.5Re at 1373 K.

the aged specimen shows a small increase in strength over the annealed specimen, consistent with hardness results [14]. However, perhaps more important is the lack of work hardening observed in both specimens. While both the aged and annealed specimens reach very high total elongations, the UE is only 14.5%, 8.8%, and 7.5% for the annealed and two aged specimens, respectively. This indicates a loss of work hardening, which may lead to premature localized necking during service at high temperatures.

The sample irradiated to 0.66 dpa at 1373 K (R717) showed a large increase in strength, both YS and UTS, over the aged and annealed specimens, but not as large as that for the tests at 1073 and 1223 K. This sample also failed abruptly at only 4.4% elongation with no evidence of necking. Indeed, the SEM fractography shows that the reduction of area for this sample was only 2.9%, significantly less than that for the annealed and aged specimens (89.2% and 69.8%, respectively). This irradiated specimen was also found to have failed in a completely IG mode.

3.2. Mo–41Re

For the Mo–41Re alloy, a total of 16 tensile tests were completed. Annealed and aged specimens were tested at all temperatures. Specimens irradiated at 1073 K to 0.72 dpa, at 1073 K to 1.46 dpa, at 1223 K to 0.67 dpa, and at 1373 K to 0.66 dpa were tested. The measured mechanical properties for all tests are summarized in Table 4. Fractography has been completed on most of the Mo–41Re specimens and the quantitative results are also listed in Table 4.

3.2.1. Tests at 1073 K

Results of the tensile testing for Mo–41Re at 1073 K are shown in Table 4, while the stress–strain curves for the aged, annealed, and irradiated Mo–41Re specimens are shown in Fig. 6. The curves and mechanical properties are virtually identical for the aged and annealed samples, consistent with the hardness and resistivity results from the same samples [14]. Both curves show a slight yield drop followed by a limited Luders strain region. In addition, both samples exhibit dynamic strain aging (DSA) [17] during plastic deformation for all plastic strains greater than the Luders strain.

Two irradiated Mo–41Re samples (1073 K to 0.72 dpa) were also tested. The stress–strain curves for irradiated samples are shown in Fig. 6. Very large increases in yield and ultimate tensile stress were measured, although the irradiated Mo–41Re samples also retained a fairly high ductility for such a high strength. The results were similar to that for the irradiated Mo–47.5Re samples as the irradiated samples exhibit a very high degree of hardening over the annealed and aged conditions. However, the tensile ductility for both specimens is good (uniform elongation >5%) given the very high degree of strengthening. It is also interesting to note that no DSA was observed for the irradiated specimens.

Fractography has been performed on the Mo–41Re specimens tested at 1073 K. The nature of failure was characterized and the reduction in area measured. The results of the fractography analysis are summarized in Table 4 while the fracture surfaces for the annealed, aged, and 0.69 dpa Mo–41Re samples tested at 1073 K are shown together in Fig. 7. All samples failed via ductile rupture. The fracture surface for the irradiated Mo–41Re sample, M106 in Fig. 7, shows the classic cup and cone appearance for ductile failure. The sample failed via ductile rupture with a much higher reduction in area (58.4%) than the Mo–47.5Re samples irradiated and tested at the same conditions.

Three tests were completed at 1073 K for the samples irradiated at 1073 K to 1.46 dpa (see Fig. 6). Sample M110 showed an exceptionally large increase in strength over the aged and annealed specimens with a YS of 1264 MPa and a UTS of 1602 MPa. The sample failed abruptly with the UE and TE approximately equal at 5.1%. The other two samples (M109 and M112) underwent brittle failure before reaching the yield point at stresses of greater than 1 GPa. Fractography has not been completed, but should be performed to confirm that the mode of failure was IG in nature.

3.2.2. Tests at 1223 K

Tensile tests at 1223 K have been completed for both a Mo–41Re specimen aged at 1248 K and an annealed Mo–41Re specimen. The measured properties shown in Table 4 indicate that the annealed specimens are very slightly stronger than the specimen aged at 1248 K for 1100 h, however the results are based on only one tensile test for both the aged and annealed conditions. The stress–strain curves for the aged, annealed and irradiated specimens are shown in Fig. 8. Both unirradiated curves again show a yield drop, small Luders strain region and some limited dynamic strain aging at higher

Table 4
Tensile properties of Mo–41Re

Test temperature (K)	Sample	Condition	YS (MPa)	UTS (MPa)	Uniform elongation (%)	Total elongation (%)	Failure location	Failure type[a]	Reduction area (%)	IG/TG Fracture (%)
RT	M125	Annealed	769	900	17.2	>25				
1073	M130	Annealed	303	503	17.9	30.0	Gage	Ductile	93.5	0
	M132	Aged (1098 K)	294	500	19.2	30.6	Gage	Ductile	93.3	0
	M105	Irradiation (1073 K/0.72 dpa)	772	1130	7.7	13.4	Gage	Ductile	71.4	0
	M106	Irradiation (1073 K/0.72 dpa)	862	1180	5.5	12.6	Gage	Ductile	58.4	0
	M109[b]	Irradiation (1073 K/1.46 dpa)	–	1392	–	–	Gage			
	M110	Irradiation (1073 K/1.46 dpa)	1264	1602	5.1	5.2	Gage			
	M112[b]	Irradiation (1073 K/1.46 dpa)	–	1063	–	–	Gage			
1223	M127	Annealed	275	393	16.8	39.0	Gage	Ductile	98.8	0
	M136	Aged (1248 K)	265	398	16.8	35.1	Gage	Ductile	96.1	0
	M101	Irradiation (1223 K/0.67 dpa)	<100 MPa			<1	Gage	IG	0.1	100
	M102	Irradiation (1223 K/0.67 dpa)	765	1019	6.5	12.2	Gage	IG	15.1	100
	M104	Irradiation (1223 K/0.67 dpa)	790	987	5.4	16.3	Gage	IG	27.2	88
1373	M126	Annealed	228	275	11.7	50.5	Gage	Ductile	80.6	0
	M139	Aged (1398 K)	241	300	9.4	62.3	Gage	Ductile	91.3	0
	M117	Irradiation (1373 K/0.66 dpa)	575	754	3.5	7.5	Gage	IG	13.0	100

[a] Failure type given as ductile, intergranular (IG), transgranular (TG), or mixed (IG/TG).
[b] Sample failed before yielding.

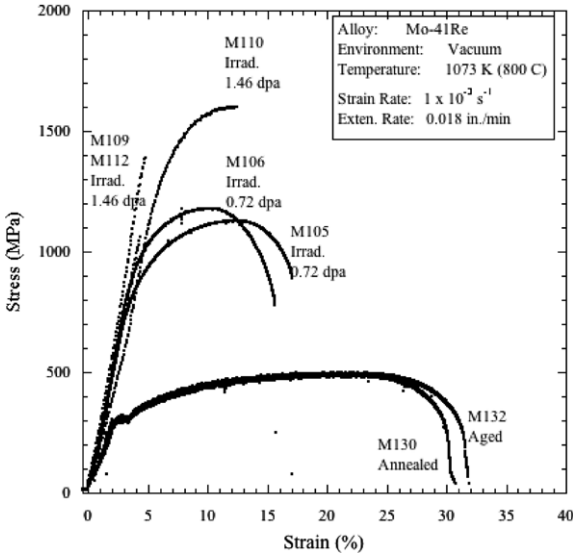

Fig. 6. Comparison of stress–strain curves for irradiated, aged, and annealed Mo–41Re at 1073 K.

extensions. The magnitude of the serrations is less than that observed for testing at 1073 K.

In addition, three Mo–41Re samples irradiated to 0.69 dpa at 1223 K were tested in vacuum at 1223 K. Sample M101 failed during the initial loading of the sample. This premature failure (<0.1% elongation) occurred at a stress of less than 100 MPa. The other two samples showed significant hardening over the aged and annealed conditions. These two specimens also show a loss in ductility, comparable to the specimens irradiated and tested at 1073 K. While the UE and TE are similar for the samples irradiated and tested at 1073 and 1223 K, the reduction-in-area is much lower for the Mo–41Re irradiated at 1223 K.

Fractography was performed on all five specimens tested at 1223 K. Both the aged and annealed specimens had an extremely high reduction of area (96.1% and 98.8%, respectively) and failed in a ductile mode. The irradiated samples M102 and M104 had a considerably lower reduction in area (15.1% and 27.2%, respectively) and showed a very distinct IG behavior. The fracture surface of irradiated sample M101 is also of interest due to the brittle failure of this specimen. This sample failed via total IG failure, similar to the Mo–47.5Re samples irradiated and tested at 1223 K.

3.2.3. Tests at 1373 K

Annealed, aged, and irradiated Mo–41Re specimens have also been tested at 1373 K. The stress–strain curves for the annealed and irradiated samples are shown in Fig. 9 (the electronic data file for the aged specimen (M139) was corrupted during testing and is not available for comparison). Aging at 1398 K for 1100 h resulted in a small

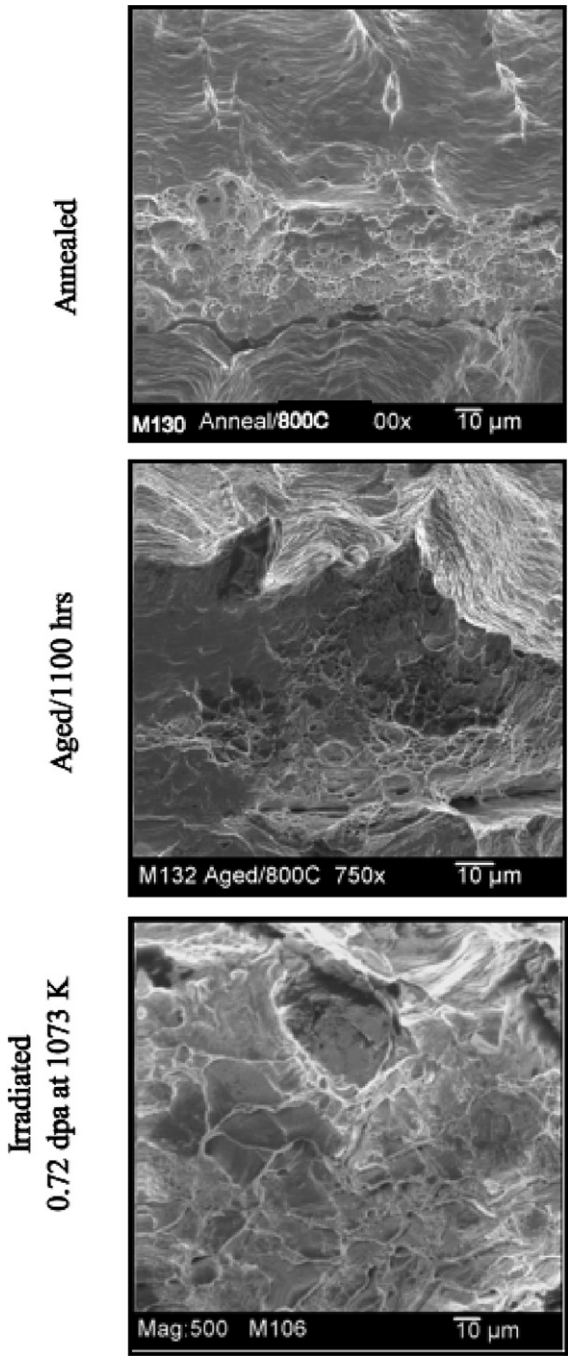

Fig. 7. Comparison of fracture surface of annealed, aged, and irradiated Mo–41Re samples tested at 1073 K.

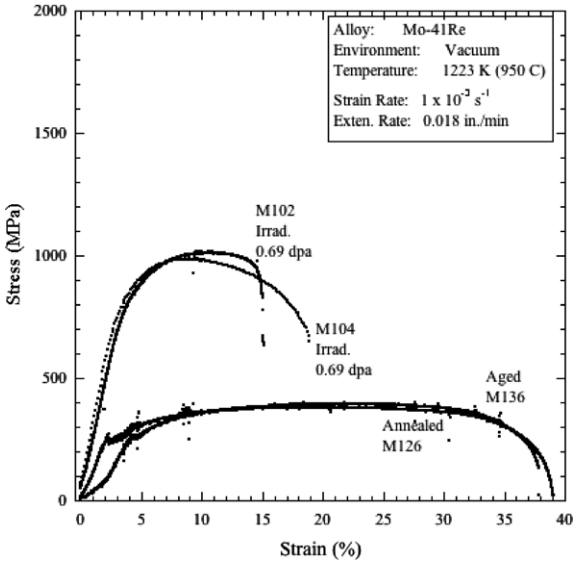

Fig. 8. Comparison of stress–strain curves for irradiated, aged, and annealed Mo–41Re at 1223 K.

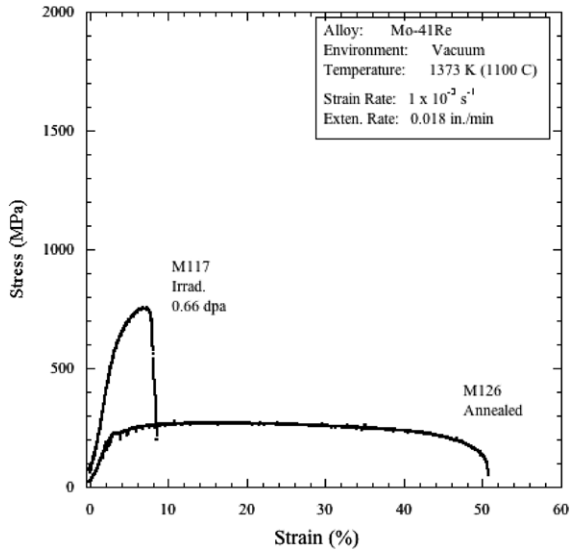

Fig. 9. Comparison of stress–strain curves for irradiated and annealed Mo–41Re at 1373 K.

degree of strengthening for tensile tests at 1373 K; this behavior is in contrast to the room temperature hardness results reported earlier [14], although both samples reached very high total elongations. Furthermore, compared to the Mo–41Re behavior at 1073 and 1223 K, both specimens tested at 1373 K also had a relatively low uniform elongation and exhibited low work hardening, similar to the Mo–47.5Re tests at the same temperature. A sample irradiated at 1373 K to 0.66 dpa has been tested. A moderately high degree of radiation hardening was observed (although less than in specimens irradiated at lower temperatures) along with a significant drop in ductility.

The results of the quantitative fractography of the annealed, aged, and irradiated specimens are shown in Table 4. As expected, the annealed and aged specimens show very high reductions in area, consistent with the high TE observed for both specimens. The irradiated specimen had very little reduction in area (13.0%) and exhibited total IG failure.

4. Discussion

Both Mo–Re alloys of this study exhibited a high degree of strengthening due to irradiation at all three temperatures, with a concurrent loss of ductility. The increases in YS and UTS from the annealed condition for Mo–47.5Re were greater than that observed for Mo–41Re irradiated to the same conditions. This higher irradiation-induced strengthening in Mo–47.5Re may be due to the higher Re content and phase instabilities. In the aged Mo–47.5Re samples, the formation of sigma, σ, and chi, χ, phases was observed after 1100 h, whereas no precipitation has been observed in the aged Mo–41Re samples [14]. Under irradiation, the higher Re content is expected to lead to more precipitation, radiation-induced segregation, and transmutation (primarily the formation of Os from Re). All these factors would lead to enhanced strengthening of Mo–47.5Re over Mo–41Re, consistent with these results. In this section, the mechanism for the observed strengthening and embrittlement are examined.

A number of studies reported in the open literature have examined radiation-induced changes in Mo alloys with varying Re contents. Fabrietsiev and Pokrovsky [9] examined the tensile properties in Mo–Re alloys (with Re varying from 0.5% to 47%) irradiated over a range of temperatures in either the mixed spectrum of the SM-2 reactor or the fast spectrum of the BOR-60 reactor. Severe embrittlement and brittle fracture was observed in the 573–873 K temperature regime. Some ductility was retained for irradiations and tests between 973 and 1073 K. Hasegawa et al. [18] found that a Mo–5Re alloy irradiated in FFTF at 646–1073 K also exhibited a very high degree of hardening, but did not undergo brittle fracture.

Gorynin et al. [19] irradiated a Mo–7Re-0.1Hf alloy at 1073 K to several dpa and found significant

hardening and a large reduction in sample ductility, consistent with the results of this and other studies. Scibetta et al. [20] found severe fracture toughness embrittlement in Mo–5Re irradiated at 320–723 K to only 0.2 dpa. Loss of fracture toughness may be a significant concern for the specimens irradiated in this study as well, given the very high strengths observed at all temperatures. For BCC metals, there is a linear relationship between the hardening and the shift in the ductile–brittle transition temperature (DBTT). This Ludwig–Davidenkov relationship has been observed in irradiated V–Cr–Ti alloys [21], where increases of 500–800 MPa in yield strength (similar to what has been observed in this study) corresponded to a 300–500 K shift in DBTT. Using the Ludwig–Davidenkov relationship and the fracture toughness of unirradiated Mo–Re alloys, matrix strengths above ~1000 MPa are expected to produce fracture toughness embrittlement.

While the comparisons with Mo alloys with low Re content show similar trends to the results from this study, a direct comparison with irradiation damage in Mo–47.5Re or Mo–41Re is more meaningful. Only the study of Fabrietsiev and Pokrovsky [9] contains data that is directly comparable to the results of this study. Fabrietsiev and Pokrovsky irradiated Mo–47Re to approximately 2 dpa in the mixed neutron spectrum of the SM-2 reactor at approximately 600 K. In addition, Mo–47Re was also irradiated to 5–10 dpa at 700–1100 K in the fast neutron spectrum of the BOR-60 reactor, which, while not the same spectra as this study, is more directly applicable to space reactor applications. The results of Fabrietsiev and Pokrovsky are plotted in Fig. 10 as a function of irradiation and test temperature. The data at 0.72 dpa from the present study are also plotted for comparison. Due to the uncertainties associated with the Mo–47.5Re irradiated to 1.46 dpa (bent loading pins and failure at the sample hole), these data are not shown. For consistency with the Mo–47.5Re and clarity, the data associated with the brittle failure of the Mo–41Re irradiated to 1.46 dpa are also not shown. The results for Mo–47.5Re at 1073 K to 0.72 dpa are in excellent agreement with the data from the open literature. Although not shown in the plot, the strengths for the brittle failure for the Mo–41Re at 1.46 dpa at 1073 K are consistent with the data trends shown in Fig. 10. While the damage level is considerably lower for the samples irradiated in HFIR, they were also irradiated in a mixed neutron spectrum, which will enhance transmutation of Re

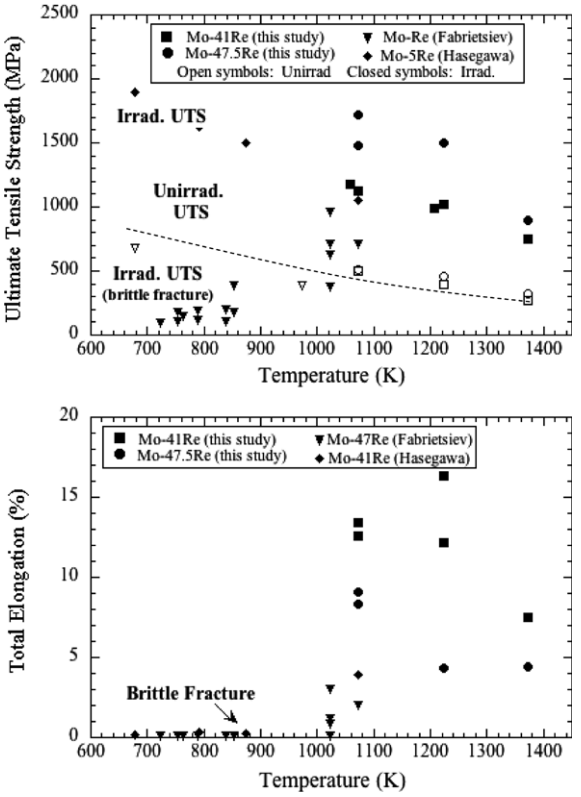

Fig. 10. Comparison of mechanical properties for Mo–41Re and Mo–47.5Re samples irradiated to 0.72 dpa with results of Fabrietsiev and Pokrovsky [9] for irradiated Mo–47Re alloys.

(and resulting precipitation). This difference will accelerate radiation-induced hardening, consistent with the results shown in Fig. 10. The ductility data for the samples irradiated to 0.72 dpa also suggest that the irradiations at temperatures above 1073 K do not suffer from the low temperature embrittlement phenomenon observed by Fabrietsiev and Pokrovsky at temperatures below 973 K. The present study, however, is the first where the irradiation of Mo–Re alloys has been conducted above 1073 K and the increasing IG nature of the fracture in samples tested with increasing temperature suggests that these alloys have poor intergranular strength following high temperature irradiation. This observation is confirmed by the brittle failure of the samples irradiated to 1.46 dpa. Further analysis of the fractography and tensile properties may provide some insight into the mechanisms of failure in these irradiated Mo–Re alloys.

The fracture surface for the Mo–47.5Re and Mo–41Re are compared in Fig. 11 as a function of alloy and irradiation/test temperature. All irradiated

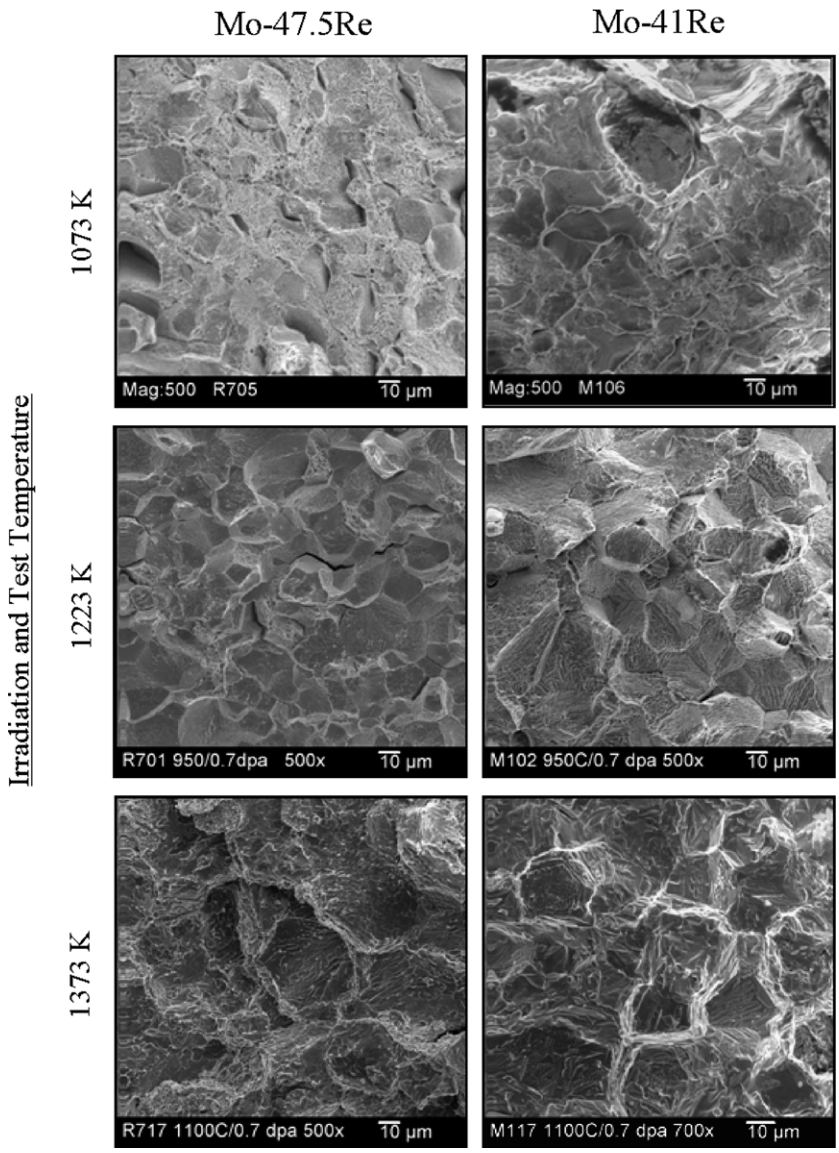

Fig. 11. Comparison of fracture surface features as a function of irradiation and test temperature for Mo–47.5Re and Mo–41Re irradiated in HFIR for one cycle (~0.7 dpa).

samples, except the Mo–41Re irradiated at 1073 K, exhibited evidence of IG failure. The IG facets appear at lower temperatures in the Mo–47.5Re alloy than the Mo–41Re alloy. Further, at each irradiation and test temperature above 1073 K, the grain facets appear coarser in the Mo–47.5Re than in the Mo–41Re with the roughness increasing with increasing irradiation temperature. Fractography of the samples irradiated to 1.46 dpa is needed to determine if the same trends also hold with increasing dose.

The IG facets found in the fractography analysis of the Mo–47.5Re specimens irradiated at all three temperatures to 0.66–0.72 dpa indicate that grain boundary embrittlement is severe under these irradiation conditions. Indeed, the fraction of IG features increases with increasing irradiation and test temperature for both alloys, although the Mo–41Re alloy remained ductile after irradiation to 0.72 dpa at 1073 K. In a similar fashion, the reduction in area decreases with increasing irradiation temperature for both alloys. Again, Mo–41Re retained a higher

level of ductility than Mo–47.5Re after 0.72 dpa at 1073 K, but was brittle after 1.46 dpa at the same temperature. However, most acceptable structural alloys have reduction in area greater than 20% and less than 10% IG failure. This raises concern about the suitability of Mo–47.5Re and Mo–41Re for irradiated structural applications at all temperatures (1073–1373 K) examined in this study.

The trends in both the qualitative and quantitative fractography may be related to radiation-induced segregation (RIS) and/or transmutation, which could lead to precipitation during irradiation. The formation of precipitates could result in the increasing degree of IG fracture observed in this program. This potential form of degradation has been observed in vanadium and vanadium alloys already [22] and must be considered further. The influence of RIS and transmutation on embrittlement will be discussed in greater detail in the following sections.

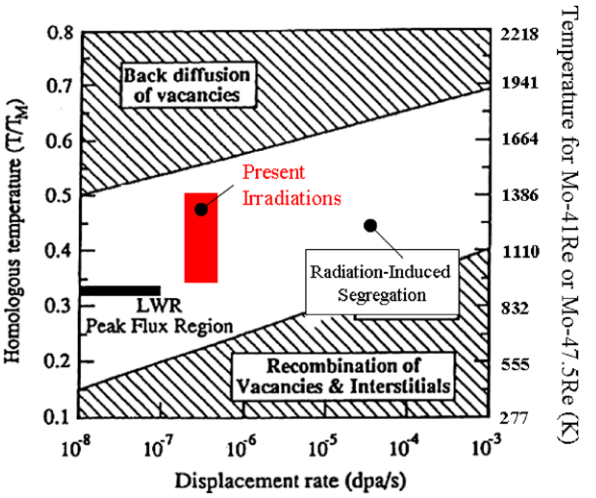

Fig. 12. Homologous temperature vs. flux, showing the regimes where RIS is most pronounced (reproduced from Ref. [23]). The region for these irradiations on Mo–Re alloys is also indicated.

4.1. Radiation-induced segregation and precipitation

Radiation-induced solute segregation refers to the redistribution of elements (solute or interstitial impurities) under irradiation. The motion of the high concentrations of radiation-induced vacancies and interstitials to defect sinks such as grain boundaries or dislocation loops will result in localized enrichment or depletion if any atom has a preferential association with interstitials or vacancies, respectively.

The degree of segregation will vary with temperature, dose rate, and dose. A schematic of the segregation process is shown in Fig. 12. The displacement rate and temperature regime for the irradiations of this program are superimposed in Fig. 12 while the temperature for Mo–Re alloys is shown on the right-hand axis. At low temperatures ($<0.3T_m$), defect mobility is low and defects are more likely to be lost due to mutual recombination or at defects such as dislocation loops, limiting the amount of RIS. At higher temperatures ($>0.5T_m$), thermal defect concentrations are large. In this high temperature regime, the driving force for segregation (a defect concentration gradient) is reduced and vacancy back diffusion of segregated species tends to retard the segregation process. At intermediate temperatures, point defects generated by radiation diffuse to defect sinks. Preferential association between defects and a particular alloy element will pair a net flux of the alloying element to the defect fluxes causing a depletion or enrichment of elements at the grain boundary or other defect sinks. The degree of RIS in the Mo–Re alloys irradiated in this program should be significant and reach a peak between 1200 and 1400 K.

Modeling and measurement of RIS in Mo–Re alloys has been discussed by Erck and Rehn [24,25], previously. Predictions of RIS in Mo–Re [24] indicate that Re will become enriched at defect sinks such as grain boundaries, free surfaces and dislocations (network or dislocation loops). The predictions of Erck and Rehn have also been confirmed using Rutherford-backscattering spectrometry (RBS) on Mo–41Re and Mo–45Re ion-irradiated with 1.8 MeV helium and neon ions [25]. Enrichment of Re was measured at the surface of the thin foil specimens. For the Mo–45Re alloy, segregation was observed from 1073 K to 1498 K with the maximum segregation measured at 1223 K. The amount of segregation normalized to irradiation dose is plotted in Fig. 13 as a function of irradiation temperature. The peak segregation observed for Erck and Rehn in Fig. 13 coincides with the expected region for peak RIS shown in Fig. 12. Perhaps more importantly, it is also important to note that for a Mo–47.5Re alloy, only a small amount of local Re enrichment is required to enter a regime where precipitation will occur.

Studies of the effects of neutron irradiation at high fluence on Mo–Re alloys ($\sim 1 \times 10^{23}$ n/cm^2, $E > 0.1$ MeV) at temperatures of 646–1073 K have

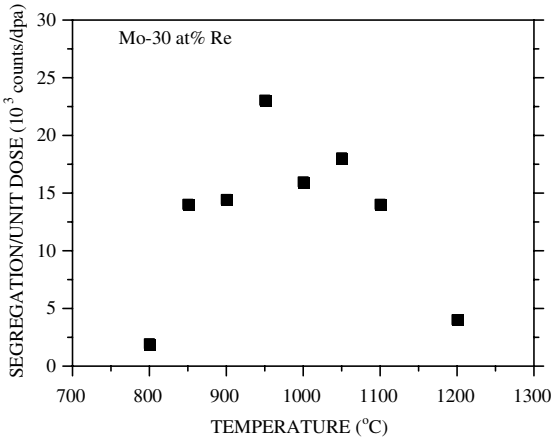

Fig. 13. The degree of segregation per dpa plotted as a function of the irradiation temperature for Mo–45Re (taken from [24]).

reported precipitation of intermetallic particles (concurrent with decreased ductility following irradiation [10,26].) This radiation-induced precipitation of both σ and χ phases has been reported in other studies as well [27,28] and is likely the result of radiation-induced segregation. Edwards et al. [29] also report neutron-induced segregation and transmutation of Re in a Mo–41Re alloy irradiated in FFTF at temperatures from 744 to 1073 K to 40 and 60 dpa. Both a χ phase and an unidentified hcp, Re-rich phase were observed.

Indeed, precipitation has already been observed in the Mo–47.5Re specimens aged at 1098, 1248, and 1398 K for 1100 h [14]. After aging at 1248 K, TEM analysis has shown χ-phase along grain boundaries in Mo–47.5Re [14]. Aging at 1398 K, resulted in a nearly continuous layer of sigma phase along grain boundaries. During irradiation, radiation-enhanced diffusion and radiation-induced segregation will both further promote Re enrichment at the grain boundaries, leading to further formation of χ or σ phases.

During irradiation, χ-phase precipitation also formed at the irradiated surface of the samples examined by Erck and Rehn [25]. Since these specimens were ion-irradiated in-situ, the irradiated and unirradiated portions of the same sample can both be examined. The microscopy of this study and others [26,29] clearly showed precipitation at both grain boundaries and within the grain matrix (presumably at dislocation loops). However, the precipitation only occurs in the irradiated portion of the sample, which confirms that the formation of χ must be due to RIS and not thermal processes. In a Mo–41Re specimen, Erck and Rehn also used energy dispersive spectroscopy (EDS) in a transmission electron microscope (TEM) to measure the composition of these precipitates and reported Re contents above 60 at.% (75 wt%), consistent with χ-phase. This observation is also consistent with the work of Edward et al. [29].

Precipitation could also result from radiation-induced transmutation [30]. Both ^{185}Re and ^{187}Re have large (n,γ) thermal energy cross-sections which lead to significant transmutation of Re to Os, although the rates of transmutation will depend on the neutron energy spectrum of the reactor and reactor position. Osmium has a lower solubility in Mo than Re (only 8% at 1273 K) and could form Mo_3Os at relatively low damage levels, leading to embrittlement. It should also be noted that Os may also undergo RIS, further enhancing precipitation, although nothing is known about Os segregation. The presence of Os could also influence irradiation creep, growth, and swelling, as noted by Garner et al. [31].

Some preliminary composition analysis was performed on the irradiated Mo–41Re specimens. Energy dispersive spectroscopy (EDS) was performed in an initial attempt to determine the amount of Os present in the irradiated sample. An EDS spectrum was acquired for both an annealed and irradiated Mo–41Re specimen. The very high residual background created from the radioactive specimen makes quantitative analysis very difficult, but a distinct Os peak was visible in the spectrum of the irradiated sample. The peak counts for Mo and Re in the annealed specimen were determined and a *k*-factor (a scaling factor to relate spectra intensities to concentrations) was determined using the Cliff–Lorimer ratio technique [32]. Assuming that the Mo concentration did not change appreciably during irradiation due to transmutation, this *k*-factor was then used to determine the Re content in the irradiated specimen. No effort was made to separate the Os and Re peaks. The results indicate that after irradiation to 0.72 dpa at 1073 K, the Mo–41Re sample has transmuted to approximately Mo–24Re–17Os. It should be noted that due to the low signal-to-background ratio and need to separate Re and Os peaks, the uncertainty on this measurement of 17% Os is very large. Nonetheless this provides and rough estimate of Os content, and the presence of a distinct Os peak indicates that transmutation may play an important role in the irradiation-induced degradation of Mo–Re alloys.

4.2. Radiation-induced segregation, precipitation, and embrittlement

In an effort to help understand the potential influence of transmutation and Os formation on phase stability, ternary Mo–Re–Os phase diagrams have been constructed at several different temperatures. Each ternary phase diagram was constructed from the Mo–Re, Mo–Os, and Os–Re binary diagrams [33]. The diagram shown in Fig. 14 is an isothermal section of the ternary at 1073 K.

The composition change for Mo–47.5Re and Mo–41Re alloys has also been estimated for irradiation in the mixed thermal spectrum of HFIR based on the work of Greenwood and Garner [30]. These compositions are plotted on the ternary phase diagrams at distinct damage levels (0–10 dpa) for both Mo–47.5Re and Mo–41Re using the circles and diamonds, respectively. The composition changes expected for the same alloys irradiated in a fast spectrum are much different than a mixed thermal spectrum and have also been calculated (shown in Fig. 14 as the open symbols). Note that transmutation in the fast spectrum is considerably reduced from the mixed spectrum, although still an important factor. This is expected, as the most significant absorption cross sections for Re are in the thermal neutron regime.

The phase diagram predicts that phase transformations due to transmutation alone will occur at fairly low damage levels at all temperatures in the HFIR spectrum (as transmutation is independent of temperature). Indeed, the formation of Mo_3Os is expected by 1 dpa for Mo–47.5Re and about 1.5 dpa for Mo–41Re due to transmutation alone (i.e., ignoring RIS). In a fast spectrum, this dose increases to about 8 dpa for Mo–47.5Re and 9 dpa for Mo–41Re.

The very preliminary EDS information for the Mo–41Re irradiated at 1073 K to 0.72 dpa indicates that the Os concentration is approximately 17 wt%. This data point is noted on the ternary phase diagram with the star. This measurement is above the predicted value of 10.5 wt% at that damage level

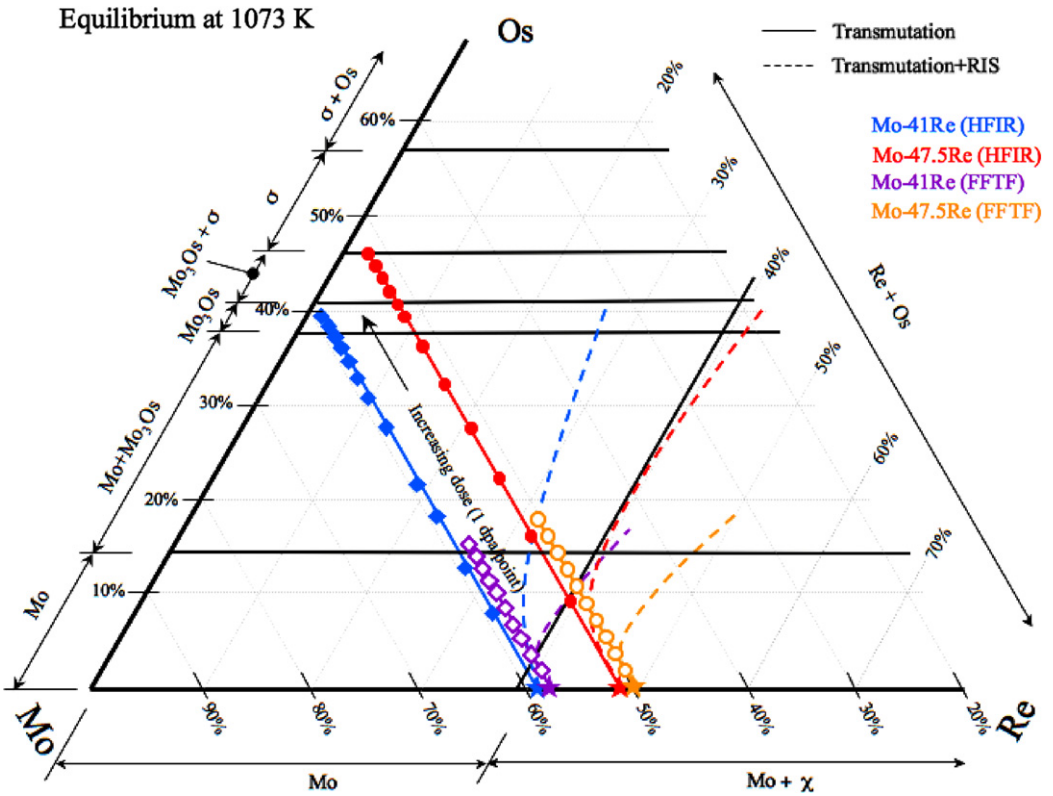

Fig. 14. Ternary phase diagram for Mo–Re–Os at 1073 K. The concentration is plotted as a function of damage level for Mo–47.5Re (circles) and Mo–41Re (diamonds) in the spectrum for both HFIR (closed symbols) and FFTF (open symbols). The dashed lines represent the best estimate of the influence of RIS.

and indicates that bulk phase transformations may have already occurred. However, it is again important to note that the high residual background in the measurement and peak overlap will inflate the measured Os content.

However, the dose required for precipitation will be less than these levels as RIS will drive both Re and Os to enrich at defect sinks during irradiation. Lines have been added to show the potential influence of RIS on phase stability. The dashed lines in Fig. 14 represent the best estimates of the expected direction and magnitude of segregation based on the results of Erck and Rehn [24]. While these are only estimates, they do indicate that local concentrations may be considerably different than bulk composition and that precipitation is feasible.

The ternary phase diagram for irradiation in Fig. 14 also indicates that after irradiation, the alloy is likely to have two-phase regions where solid-solution Mo–Re and χ phase are both present. For irradiation at higher temperatures, the grain boundary region (or areas surrounding dislocations) may be comprised of three phases including solid-solution Mo–Re, Mo_3Os and Mo–Re σ or χ phases. The presence of grain boundary precipitation could also explain both the continued degradation with increasing irradiation temperature and the nature of the fracture appearance.

As described above, second phases will begin to form and build up along grain boundaries during irradiation. With increasing bulk Re content, the amount of transmutation to Os and the degree of segregation of Re and Os will increase, leading to greater thicknesses of second phase regions at the grain boundary. Similarly, with increasing irradiation temperature, the degree of segregation and degree of precipitation will increase. Increasing dose up to a few dpa will also increase the degree of segregation (until it saturates) and the degree of precipitation. The second-phases that form in Mo–Re alloys (σ, χ, and/or Mo_3Os) are all strong but brittle phases. During deformation, these areas are likely to deform less than the surrounding matrix, which could lead to IG failure. However, at a critical second-phase thickness, the precipitate layer and grain boundary region will become more brittle than the surrounding grain matrix. At this point, the sample will tear at the matrix–precipitate interface rather than at the grain boundary itself. This mode of failure is shown schematically in Fig. 15.

In both alloys, the percent IG increased with increasing irradiation temperature, as shown in

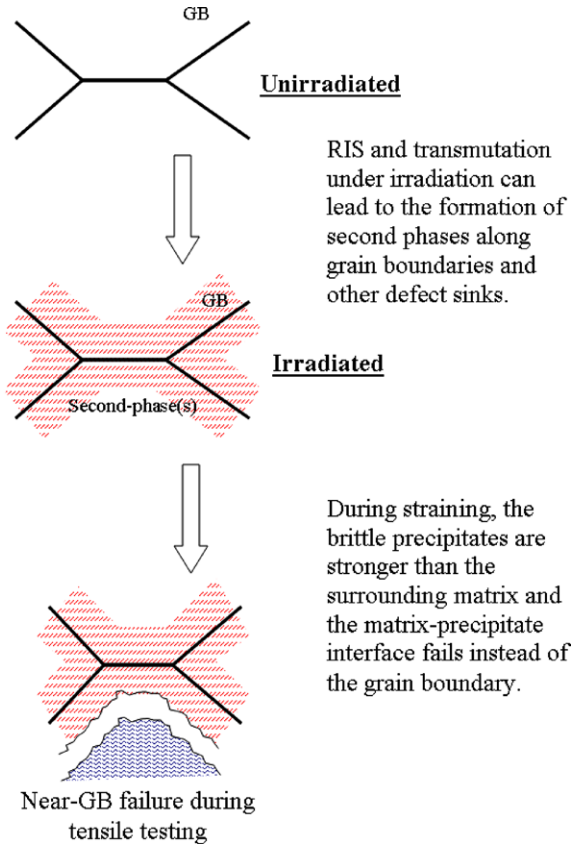

Fig. 15. Schematic illustration of the influence of RIS, transmutation, and precipitation on the tensile behavior of Mo–Re alloys.

Fig. 11. Furthermore, for both alloys the grain facets observed on the fracture surface appear rougher with increasing temperature. Both observations are consistent with the formation of thicker grain boundary layers with increasing irradiation temperature, as described above. In addition, the Mo–47.5Re became susceptible at a lower temperature than Mo–41Re and also had a higher degree of IG failure at 1223 and 1373 K than Mo–47.5Re. This is also consistent with a precipitation-induced embrittlement mechanism as the degree of transmutation and segregation are greater in the Mo–47.5Re alloy than the Mo–41Re alloy.

Alternatively, the precipitation of Re and Os-rich phases at defect sinks like dislocation loops must also be considered. In this case, the σ, χ, and/or Mo_3Os brittle second-phases forming in Mo–Re alloys will form at many locations distributed throughout the grain interior, similar to that observed by [18,25,29] and result in large increases in strength. In turn, this would leave the grain boundary region as the weakest point during defor-

mation, resulting in embrittlement. While precipitation of second-phases at dislocation loops could result in the observed embrittlement, this cannot explain the trends in fractography with dose and temperature as observed in Fig. 11. A combination of matrix hardening and precipitation with grain boundary segregation and precipitation may be the true mechanism for embrittlement in Mo–Re alloys.

While this mechanism appears plausible, a more detailed analysis of the irradiated microstructure of the irradiated Mo–Re alloys using transmission electron microscopy (TEM) is needed to confirm this mode of failure. If this information can be obtained, the mode of failure in Mo–47.5Re and Mo–41Re can be confirmed. Further analysis with TEM will also provide insight into precipitation within the grains and if there are any denuded zones or other features that could impact hardening and embrittlement.

This analysis could be a critical step in creating a Mo–Re alloy, which is resistant (or at least tolerant) to radiation-induced changes. A simple reduction in Re content from the commercially available Mo–41Re and Mo–47.5Re to a more moderate 25 wt% Re may considerably improve the alloys performance under irradiation. A lower Re content will improve irradiation-performance by reducing the degree of thermal precipitation by moving farther away from the solubility limit of Re in Mo, by reducing the driving force for radiation-induced segregation, and thereby reducing the degree of radiation-enhanced precipitation and embrittlement, and by reducing the degree of transmutation, which in turn, further reduces segregation of Os and precipitation of Os-bearing phases.

5. Summary and conclusions

A series of capsules were irradiated in HFIR, containing specimens of Mo–47.5Re and Mo–41Re. The capsules were designed for irradiation at 1073, 1223, or 1373 K. Post-irradiation examination was completed on the Mo–47.5Re samples irradiated to ~0.7 dpa at all three temperatures and samples irradiated to 1.4 dpa at 1073 K. Tensile testing after irradiation at all temperatures and damage levels shows an exceptional amount of strengthening (with UTS values over 1.5 GPa) and a loss in ductility compared to the aged or annealed conditions. The fracture surfaces reveal intergranular failure. Both factors indicate that fracture toughness degradation may be a key issue for this alloy under these irradiation conditions.

For the Mo–41Re and Mo–47.5Re alloys, annealed and aged specimens were tested at all three temperatures with no changes due to aging observed. Samples irradiated to 0.7 dpa at all three temperatures were tested, as have samples irradiated to 1.4 dpa at 1073 K. The specimens irradiated and tested at 1073 K showed a large increase in strength from the aged and annealed conditions, while the uniform and total elongations were reduced from the annealed condition. Fractography revealed that failure in Mo–41Re was via ductile rupture while Mo–47.5Re showed evidence of IG failure. Irradiation at 1223 and 1373 K to 0.7 dpa resulted in a high degree of hardening and grain boundary failures. Irradiation at 1073 K to 1.46 dpa resulted in a highly brittle failure typical of IG embrittlement.

The irradiated specimens of both Mo–41Re and Mo–47.5Re also exhibit intergranular failure with the severity increasing with increasing irradiation temperature. This embrittlement has been attributed to the combined effects of radiation-induced segregation and transmutation. Both factors could result in precipitation of second-phases at grain boundaries, leading to embrittlement. Understanding this form of high temperature embrittlement also opens the possibility of designing a more radiation-tolerant Mo–Re alloy by simply lowering the Re content.

Acknowledgements

The authors would like to thank J.L. Bump, J.E. Hack, E.V Mader, R.J. Nelson, and G.A. Newsome of the Naval Reactors Prime Contractor Team for many helpful technical discussions and guidance. The authors would also like to thank L.L. Snead, C.E. Duty, and especially F.A. Garner and F.W. Wiffen for many helpful discussions. Experiments involving reactor-irradiated materials are complex and require assistance from many different people. The authors would like to thank E. Ohriner, J. Mayotte, M. Williams, J. McDuffee, B. Sitterson, G. Hirtz, R, Stoller, S. Meyers, P. Bishop, J. Bailey, H. Phillips, P. Tedder, L. Gibson, J. Gardner, and R. Jones for their assistance. This work was performed under the sponsorship of NASA's Project Prometheus and directed by the US Department of Energy/National Nuclear Security Administration (DOE/NNSA) Naval Reactors. Opinions and conclusions drawn by the authors are not endorsed by DOE/NNSA Naval Reactors. ORNL

is managed for DOE by UT-Battelle, LLC, under Contract DE-AC-05-00OR22725.

References

[1] J.T. Busby, E.K. Ohriner, L.L. Snead, F.W. Wiffen, S.J. Zinkle, R.F. Luther, R.W. Buckman Jr., R.E. Gold, in: Proceedings of the Space Nuclear Conference 2005, San Diego, California, June 5–9, 2005.
[2] G.A. Geach, J.E. Hughes, in: F. Benesovsky (Ed.), 2nd Plansee Seminar, Pergamon, London, 1956.
[3] R.I. Jaffee, C.T. Sims, J.J. Harwood, in: F. Benesovsky (Ed.), 3rd Plansee Seminar, Springer-Verlag, Vienna, 1959.
[4] D.J. Maykuth, F.C. Holden, R.I. Jaffee, in: B.W. Gonser (Ed.), Electrochemical Society Symp. Rhenium, Elsevier, New York, 1962, p. 125.
[5] J.G. Booth, R.I. Jaffee, E.I. Salkovitz, in: F. Benesovsky (Ed.), 5th Plansee Seminar, Springer-Verlag, Vienna, 1959.
[6] L.B. Lundberg, E.K. Ohriner, S.M. Tuominen, E.P. Whelan, in: Physical Metallurgy and Technology of Molybdenum and Its Alloys, AMAX, Greenwich, CT, 1985, p. 71.
[7] A. Kumar, B.L. Eyre, Proc. Roy. Soc. Lond. A 370 (1980) 431.
[8] J. Wadsworth, T.G. Nieh, J.J. Stephens, Dilute Mo–Re alloys – a critical evaluation of their comparative mechanical propertiesScripta Metallurgia, 20, Pergamon, 1986, p. 637.
[9] S.A. Fabritsiev, A.S. Pokrovsky, J. Nucl. Mater. 252 (1998) 216.
[10] A. Hasegawa, K. Ueda, M. Satou, K. Abe, J. Nucl. Mater. 258–263 (Part 1) (1998) 902.
[11] T.A. Gabriel, B.L. Bishop, F.W. Wiffen, Calculated irradiation response of materials using fission reactor spectra, ORNL Report, ORNL/TM-6361, Oak Ridge National Laboratory, Oak Ridge, TN, August 1979.
[12] K. Farrell, T.S. Byun, J. Nucl. Mater. 318 (2003) 274.
[13] L.L. Snead, A.M. Williams, A.L. Qualls, in: M.L. Grossbeck, T.R. Allen, R.G. Lott, A.S. Kumar (Eds.), ASTM STP 1447, ASTM International, West Conshoshocken, PA, 2004, p. 623.
[14] K.J. Leonard, J.T. Busby, S.J. Zinkle, R. Baranwal, J. Hack, T.M. Angeliu, Y. Ballout, J. Nucl. Mater., these Proceedings, doi:10.1016/j.jnucmat.2007.03.025.
[15] Standard Test Method for Tension Testing of Metallic Materials, ASTM Standard E8-04, ASTM Standards Online, American Society for Testing and Materials, Philadelphia, PA, 2001.
[16] J.T. Busby, K.J. Leonard, S.J. Zinkle, Effects of Neutron Irradiation on Refractory Metal Alloys, ORNL/LTR/NR-PROM/05-38, 2005.
[17] R.B. Schwarz, L.L. Funk, Acta Metall. 33 (1985) 295.
[18] A. Hasegawa, K. Abe, M. Saitou, C. Nama, J. Nucl. Mater. 225 (1995) 259.
[19] I.V. Gorynin, V.A. Ignatov, V.V. Rybin, S.A. Fabritsiev, V.A. Kazakov, V.P. Chakin, V.A. Tsykanov, V.R. Barabash, Y.G. Prokofyev, J. Nucl. Mater. 191–194 (1992) 421.
[20] M. Scibetta, R. Chaouadi, J.L. Puzzolante, J. Nucl. Mater. 283–287 (2000) 455.
[21] A. Rowcliffe, private communication, 2005.
[22] S. Ohnuki, H. Takanashi, K. Shiba, A. Hishinuma, J.E. Pawel, F.A. Garner, J. Nucl. Mater. 218 (1995) 217.
[23] P.L. Andresen, F.P. Ford, S.M. Murphy, J.M. Perks, in: Proceedings of Fourth International Symposium on Environmental Degradation of Materials in Nuclear Power Systems-Water Reactors, Jekyll Island, GA, August 1989, NACE, Houston, 1990, p. 1.
[24] R.A. Erck, L.E. Rehn, J. Nucl. Mater. 168 (1989) 208.
[25] R.A. Erck, L.E. Rehn, Philos. Mag. A 2 (1) (1990) 29.
[26] Y. Nemoto, A. Hasegawa, M. Satou, K. Abe, Y. Hiraoka, J. Nucl. Mater. 324 (1) (2004) 62.
[27] F.A. Garner, L.R. Greenwood, D.J. Edwards, J. Nucl. Mater. 212–215 (1994) 426.
[28] G.A. Cottrell, J. Nucl. Mater. 334 (2004) 166.
[29] D.J. Edwards, F.A. Garner, D.J. Gelles, J. Nucl. Mater., submitted for publication.
[30] L.R. Greenwood, F.A. Garner, J. Nucl. Mater. 212–215 (1994) 635.
[31] F.A. Garner, M.B. Toloczko, L.R. Greenwood, C.R. Eiholzer, M.M. Paxton, R.J. Puigh, J. Nucl. Mater. 283–287 (2000) 380.
[32] G. Cliff, G.W. Lorimer, J. Microsc. 133 (1984) 203.
[33] T.B. Massalski (Ed.), Binary Alloy Phase Diagrams, ASM International, Metals Park, OH, 1986, p. 1615, 1623, 1806.